

See discussions, stats, and author profiles for this publication at: <https://www.researchgate.net/publication/339083276>

Evaluation and Projection of Regional Climate over East Asia in CORDEX–East Asia Phase I Experiment

Article in *Asia-Pacific Journal of the Atmospheric Sciences* · February 2020

DOI: 10.1007/s13143-020-00180-8

CITATIONS

2

READS

215

11 authors, including:



Gayoung Kim

Ulsan National Institute of Science and Technology

13 PUBLICATIONS 68 CITATIONS

[SEE PROFILE](#)



Dong-Hyun Cha

Ulsan National Institute of Science and Technology

72 PUBLICATIONS 1,130 CITATIONS

[SEE PROFILE](#)



Changyong Park

Ulsan National Institute of Science and Technology

26 PUBLICATIONS 343 CITATIONS

[SEE PROFILE](#)



Chun-Sil Jin

Korea Institute of Nuclear Safety

22 PUBLICATIONS 369 CITATIONS

[SEE PROFILE](#)

Some of the authors of this publication are also working on these related projects:



Korean NWP [View project](#)



This work was funded by the Korea Meteorological Administration Research and Development Program under Grant RACS 2010-4012, and CATER 2012-3100 and 2012-3083. The authors thank the two anonymous reviewers for their helpful and constructive comments. [View project](#)



Evaluation and Projection of Regional Climate over East Asia in CORDEX-East Asia Phase I Experiment

Gayoung Kim¹ · Dong-Hyun Cha¹ · Changyong Park¹ · Chun-Sil Jin² · Dong-Kyou Lee³ · Myoung-Seok Suh⁴ · Seok-Geun Oh⁴ · Song-You Hong⁵ · Joong-Bae Ahn⁶ · Seung-Ki Min⁷ · Hyun-Suk Kang⁸

Received: 2 October 2019 / Revised: 27 December 2019 / Accepted: 23 January 2020
© Korean Meteorological Society and Springer Nature B.V. 2020

Abstract

This study investigates the performance of simulated precipitation and estimates future changes in precipitation in CORDEX-East Asia Phase I. In the Historical experiment (1981–2005), a global climate model used as a lateral boundary condition does not realistically simulate the timing and intensity of the East Asian summer monsoon. Hence, it overestimates precipitation over East Asia. Generally, the results of the regional climate models also show similar bias characteristics to that of the large-scale forcing data. The individual biases of the regional climate model vary according to a model configuration, such as physical parameterization schemes. However, when bias correction is applied to data, the spatial variability and spatial correlation of the long-term mean precipitation become similar to the observations, and the annual cycle of precipitation is much improved. The two future experiments in the mid-twenty-first century period (2025–2049), show that mean and extreme precipitation amounts increase over the Korean Peninsula and northern China compared to the frequency of wet days. The increment of the low-level water vapor in all seasons can be attributed to the increased precipitation amounts; moreover, the East Asian summer monsoon is enhanced in mid-latitudes and lasts longer in summer owing to the strengthened western North Pacific Subtropical High. The increasing southerly wind from the East Asian summer monsoon over eastern China and the Korean Peninsula results in favorable conditions for the increase in precipitation.

Keywords CORDEX-East Asia · HadGEM2-AO · Multi-RCMs · East Asian summer monsoon · Bias correction

Responsible Editor: Kyong-Hwan Seo.

✉ Dong-Hyun Cha
dhcha@unist.ac.kr

¹ Ulsan National Institute of Science and Technology, Ulsan, Republic of Korea

² Korea Institute of Nuclear Safety, Daejeon, Republic of Korea

³ Korea Meteorological Administration, Seoul, Republic of Korea

⁴ Kongju National University, Gongju, Republic of Korea

⁵ Korea Institute of Atmospheric Prediction Systems, Seoul, Republic of Korea

⁶ Pusan National University, Busan, Republic of Korea

⁷ Pohang University of Science and Technology, Pohang, Republic of Korea

⁸ National Institute of Meteorological Sciences, Seogwipo, Republic of Korea

1 Introduction

Producing accurate climate change scenarios is essential for coping with weather-related natural disasters that have become more intense and frequent in recent years (Stocker et al. 2014). Global climate models (GCMs) have been widely used to estimate future climate change information. However, it is difficult for GCMs to represent the efficacy of local-to-regional-scale forcing such as land surface characteristics and complex topography owing to limitations in the details of climate information directly from GCMs with coarse resolution (Im et al. 2017). Regional climate models (RCMs) have been used to provide detailed climate information to compensate for the limitations of GCMs. RCMs have been able to resolve small-scale atmospheric circulations embedded within the large-scale ones simulated by GCMs since the late 1980s (Giorgi and Mearns 1999; Wang et al. 2004; Prudhomme et al. 2012; Lee and Hong 2014; Lee et al. 2017; Mezghani et al. 2017). Moreover, considerable efforts have been made to further the

methodological and technical developments, and ever-growing computational resources have facilitated multi-decadal simulations.

Since the late 1990s, several Model Inter-comparison Projects (MIP) for RCMs have been conducted to estimate the status of regional climate simulation and provide scenarios regarding regional climate. These projects include the Regional Model Inter-comparison Project (RMIP) over Asia (Fu et al. 2005), the Modeling European Regional Climate Understanding and Reducing Errors (MERCURE) project over Europe (Christensen et al. 1997), the Project to Intercompare Regional Climate Simulation (PIRCS) over the United States (Takle et al. 1999), the International Research Institute/Applied Research Centers (IRI/ARCs) regional model inter-comparisons over South America (Roads et al. 2003), and the Arctic Regional Climate Model Inter-comparisons (ARCMIP) over the Arctic (Curry and Lynch 2002). During the 2000s, PRUDENCE (Christensen et al. 2007), and ENSEMBLES (van der Linden and Mitchell 2009) constituted significant milestones in the application of regional climate scenarios as well as for regional model development (Kotlarski et al. 2014). Within the framework of the Coordinated Regional Climate Downscaling Experiment (CORDEX) initiative, the next generation of regional climate projections is already underway (Giorgi et al. 2009). The CORDEX was established through sponsorship by the World Climate Research Programme (WCRP) to produce a quality-controlled dataset of climate change information generated by RCMs. CORDEX has a standard setting for the continent-scale domain of interest to facilitate inter-model comparison (Zou et al. 2016). The experiment has been conducted actively over 14 regions.

East Asia has a complex topography, coastline, and atmospheric phenomena at various scales (Cha and Lee 2009; Cha et al. 2011; Hong and Kanamitsu 2014). Also, East Asia is under the influence of the East Asian summer monsoon (EASM), which covers eastern China, the Korean Peninsula, Japan, and the adjacent marginal seas. Primarily, the EASM forms the quasi-stationary front around the northern boundary of the Western North Pacific Subtropical High (WNPSH), which is a significant factor causing high precipitation over the East Asian region during summer. Moreover, East Asia is regarded as being highly vulnerable to natural hazards because of the increase in climate extremes under global climate change and the large population (Stocker et al. 2014). For these reasons, several researchers have been interested in generating regional climate change scenarios over East Asia. During the early 2000s, the RMIP for Asia was established to investigate the performance of RCMs over East Asia. Nine models, including one global variable resolution model and eight limited-area models from five countries, contributed to the RMIP (Fu et al. 2005). After that, CORDEX-East Asia was founded as a descendant of the RMIP by the Korea

Meteorological Administration (KMA). Many research activities on climate related information over East Asia have been conducted using RCMs produced by CORDEX-East Asia Phase I. In Park et al. (2013), RegCM4 adequately simulated the temporal variation in precipitation and its spatial distribution over the East Asian region. Lee et al. (2014) demonstrated that increasing temperature over East Asia is distinctly coupled with intensified monsoonal precipitation. In Jin et al. (2016), RCMs from CORDEX-East Asia reasonably capture the observed inter-annual variability and climatological spatial distribution of tropical cyclone activity over the East Asian region.

Climate change scenarios generated by RCMs also include errors (Giorgi and Mearns 1999; Hall 2014). These errors not only increase uncertainties reducing the reliability of future climate change scenarios, but also negatively influence the credibility of the results for other impact studies using the scenarios (Noguer et al. 1998). Some previous studies have suggested that statistically corrected model data can increase the usability of model outputs more than using the raw model outputs (Veijalainen et al. 2010; Dosio and Paruolo 2011; Hanel and Buishand 2011; Monhart et al. 2018; Pontoppidan et al. 2018). These early studies widely used bias correction methods to reduce the impacts of systematic model errors on climate change impact assessments. Ngai et al. (2017) showed that Quantile Mapping reduced the uncertainties in simulated precipitation and temperature. Szabó-Takács et al. (2019) investigated the impacts of several bias correction methods on climate simulation for Europe and confirmed that climate classification was effectively corrected by bias correction. The effects of bias correction on the precipitation trend over China were also assessed by Ding et al. (2007). As yet, no research has been conducted to estimate future changes in bias-corrected precipitation data in CORDEX-East Asia Phase I.

This study aims to evaluate the performance of simulated precipitation in CORDEX-East Asia Phase I and to estimate the climate change impacts on precipitation based on the bias-corrected CORDEX-East Asia Phase I data. This paper is organized in the following manner: the CORDEX-East Asia Phase I dataset, the observational reference data, and experiments are introduced in Section 2. Section 3 presents the evaluation results for the present period and analysis of future climate change scenarios. Finally, the summary and conclusions are given in Section 4.

2 Data and Experiments

This study utilizes the daily precipitation data from five RCMs participating in the CORDEX-East Asia Phase I experiment including Hadley Centre Global Environmental Model version 3 Regional Climate Model (HadGEM3-RA), the

Regional Climate Model (RegCM), the Seoul National University Regional Climate Model (SNURCM), the Weather Research and Forecasting model (WRF), and the Global/Regional Integrated Model system (GRIMs) (Suh et al. 2012). The configurations of the five RCMs vary in combinations of physical parameterizations, vertical coordination, and dynamic framework. The configurations of RCMs are shown in Table 1, where the listed reference describes the more detailed model setup. Concerning model dynamics, HadGEM3-RA, SNURCM, and WRF are based on a non-hydrostatic dynamical core while the others (RegCM and GRIMs) are hydrostatic models. Note that all RCMs except HadGEM3-RA applied spectral nudging to improve the large-scale waves (Cha and Lee 2009). The output from the Historical and Representative Concentration Pathway (RCP) scenarios (4.5, and 8.5) runs using the Hadley Centre Global Environmental Model version 2-Atmosphere and Ocean (HadGEM2-AO), simulated by the KMA, are employed as the large-scale forcing data for all RCM simulations (Baek et al. 2013). HadGEM2-AO is composed of an atmospheric model with a horizontal resolution of $1.875^\circ \times 1.25^\circ$ and 38 vertical levels, the top level of which is at approximately 40 km; other components include an ocean model with a 1° horizontal resolution and 40 vertical levels (Martin et al. 2011). A historical run is a simulation of the recent past, which imposes changing conditions including atmospheric composition and solar forcing consistent with the observations. RCP4.5 is a scenario that stabilizes radiative forcing at $4.5 \text{ W}\cdot\text{m}^{-2}$ in the year 2100 without ever exceeding that value (Thomson et al. 2011). RCP8.5 combines relative slow income growth, high populated assumptions with modest rates of technological change and energy intensity improvements, leading to long-term high energy demand and greenhouse gas emissions in the absence of climate change policies (Riahi et al. 2011). The model domain covers 15°S - 55°N and 75°E - 160°E , including East Asia, part of Southeast Asia, and eastern India (Fig. 1).

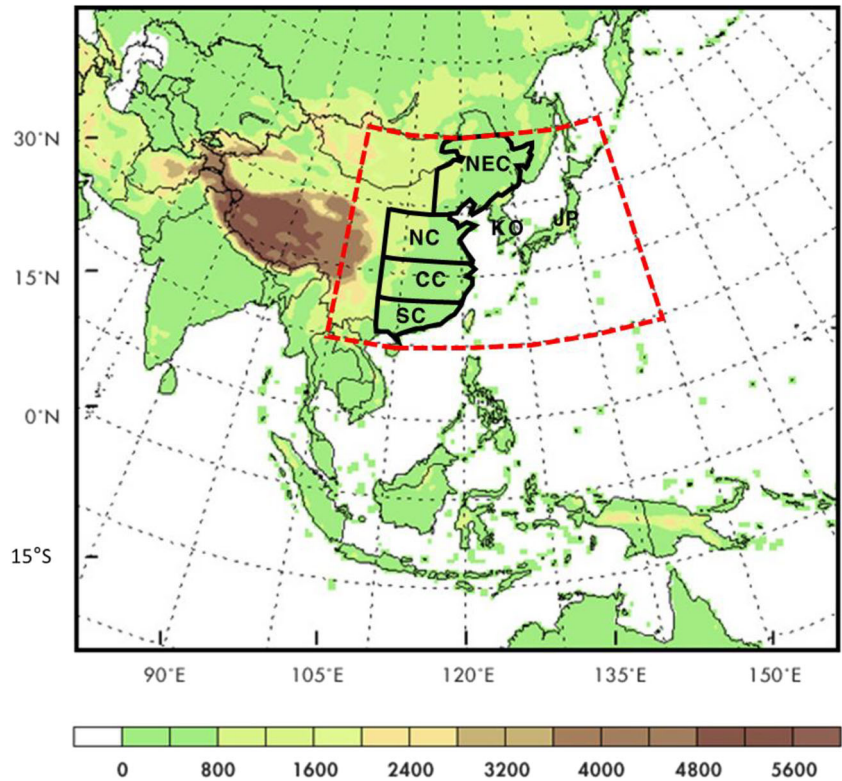
The analysis period is 25 years for both Historical (1981–2005) and RCP (2025–2049) experiments. The analysis domain covers 100° - 150°E and 20° - 50°N , focusing on the East Asian region (dashed line in Fig. 1) with a horizontal resolution of 0.44° (approximately 50 km). In this study, six sub-regions affected by the EASM are defined for additional analysis over East Asia. The sub-regions are northern China (NC), central China (CC), southern China (SC), northeastern China (NEC), the Korean Peninsula (KO), and Japan (JP).

Asian Precipitation-Highly-Resolved Observation Data Integration Towards Evaluation of the Water Resources (APHRODITE) data are used as reference data for the model evaluation and bias correction for land area. Global Precipitation Climatology Project (GPCP) data with 2.5° resolution are used as reference data for model evaluation over

Table 1 Configurations of the RCMs (Lee et al. 2004; Davies et al. 2005; Giorgi et al. 2012; Hong et al. 2013; Powers et al. 2017)

	HadGEM3-RA	RegCM4	SNURCM	WRF	GRIMs
Institution (abbreviation)	Korea Meteorological Administration / National Institute of Meteorological Sciences (KMA/NIMS)	Kongju National University (KNU)	Seoul National University / Ulsan National Institute of Science and Technology (SNU/UNIST)	Seoul National University / Pusan National University (SNU/PNU)	Yonsei University / Pohang University of Science and Technology (YSU/POSTECH)
Number of grids (Lat × Lon)	183 × 220	197 × 243	197 × 233	197 × 233	198 × 241
Radiation	General 2-stream radiation	NCAR CCM3	CCM2 package	RRTM and Dudhia	Chou's scheme
Microphysics	Single moment bulk scheme	SUBEX	ReisnerII	WSM3	Diagnostic microphysics scheme
Convection parameterization	Revised mass flux scheme	MIT-Emanuel	Kain-Fritsch II	Kain-Fritsch II	Simplified Arakawa-Schubert
Land surface model	MOSES II	CLM3	CLM3	Noah	Noah
Reference	Davies et al. (2005)	Giorgi et al. (2012)	Lee et al. (2004)	Powers et al. (2017)	Hong et al. (2013)

Fig. 1 Topography (m) in the model domain of CORDEX-East Asia Phase I. The analysis regions including the six sub-regions are demarcated by the dashed lines in red



the ocean. ERA-Interim, the reanalysis data, with 0.7° resolution, are also used as reference data for atmospheric wind and moisture analysis. The model gridded data are converted to the APHRODITE grid with 0.5° resolution using a bilinear interpolation method to compare model results with observations. The multi-model ensemble (MME) average is calculated using the unweighted averaging method.

The power transformation method (Teutschbein and Seibert 2012) is applied to the daily precipitation produced by five RCMs. Power transformation matches the coefficient of variation (CV) of model precipitation with the CV of the observed precipitation for each month by non-linear corrections in an exponential form. In this study, the parameter a_m is obtained every month using a 3-month window centered on the target month using a root-finding algorithm based on the bisection method that applies to any continuous functions for which one knows two values with opposite signs (Corliss 1977). Assume that a_m does not change even for future conditions. Thereafter, the monthly climatology of the observed precipitation is matched with the monthly climatology of the intermediary series ($P_{contr}^{*1}, P_{scen}^*$) as follows;

$$\text{Find } a_m \text{ such that } 0 = CV_m(P_{obs}(d)) - CV_m(P_{contr}^{b_m}(d))$$

$$= \frac{\sigma_m(P_{contr}^{a_m}(d))}{\mu_m(P_{contr}^{a_m}(d))} \quad (1)$$

$$P_{contr}^{*1}(d) = P_{contr}^{a_m}(d) \quad (2)$$

$$P_{scen}^{*1}(d) = P_{scen}^{a_m}(d) \quad (3)$$

$$P_{contr}^*(d) = P_{contr}^{*1} \cdot \left[\frac{\mu_m(P_{obs}(d))}{\mu_m(P_{contr}^{*1}(d))} \right] \quad (4)$$

$$P_{scen}^*(d) = P_{scen}^{*1} \cdot \left[\frac{\mu_m(P_{obs}(d))}{\mu_m(P_{contr}^{*1}(d))} \right] \quad (5)$$

Table 2 Definitions of symbols and sub-/superscripts used in the text

Symbols	
a	Parameter
CV	Coefficient of variation
(d)	Daily
μ	Mean
P	precipitation
σ	Standard deviation
Sub-/superscripts	
*	Final bias-corrected
*1	Bias-corrected in an intermediate step
contr	RCM-simulated in Historical experiment
m	Within monthly interval
obs	Observed
scen	RCM-simulated in RCP experiments

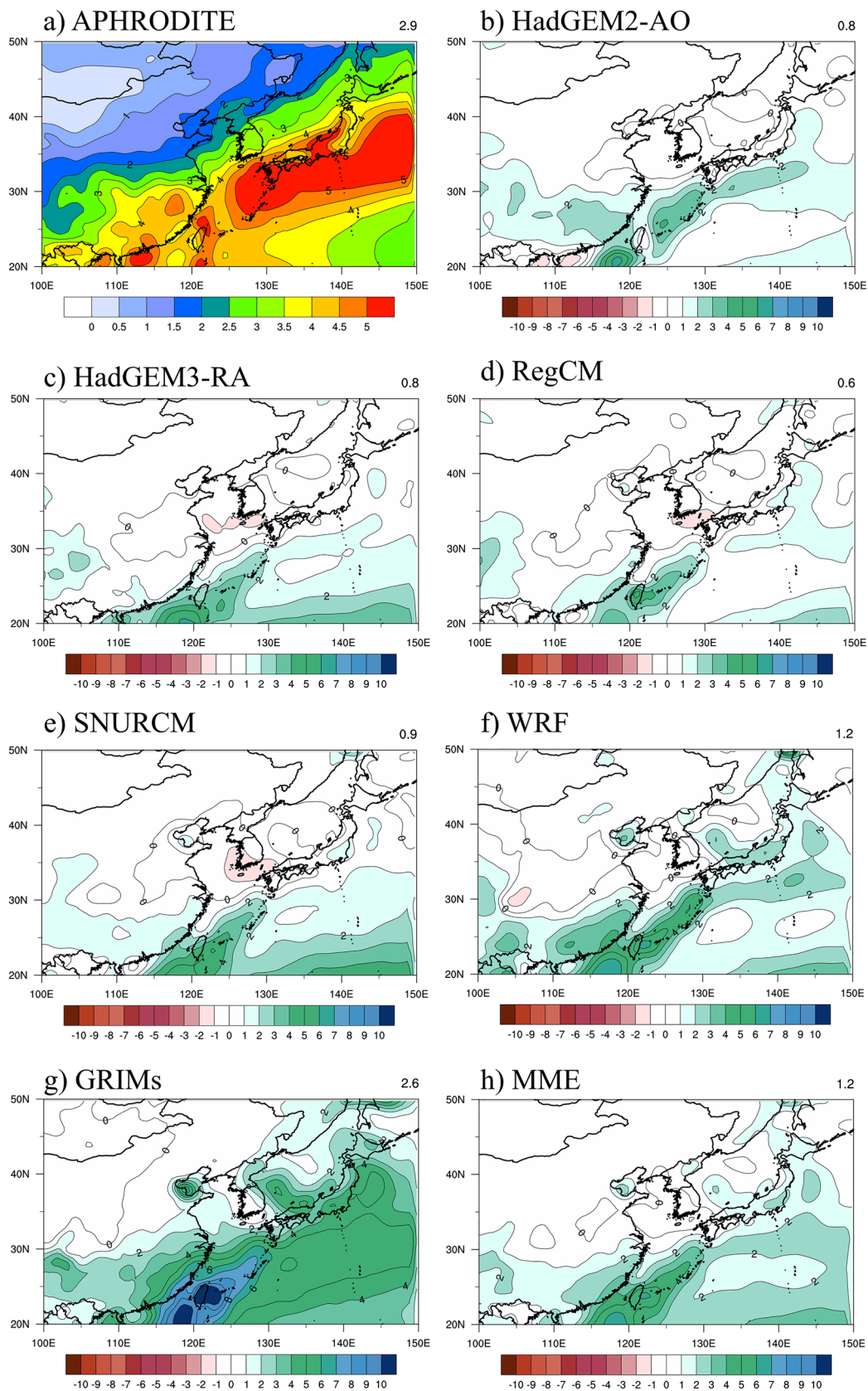


Fig. 2 25-year (1981–2005) mean precipitation ($\text{mm}\cdot\text{day}^{-1}$) of (a) APHRODITE and biases in Historical experiment from (b) the large-scale forcing data, (c–g) each RCM, and (h) MME. Numbers in the upper right corners indicate area-averaged values

Descriptions of each symbol and sub/superscripts are given in Table 2. Bias correction is not applied over the ocean owing to the lack of high-resolution daily observation.

3 Results

3.1 Evaluation of the Historical Experiment

Before the estimation of future changes in precipitation using RCMs, the evaluation for the reliability of RCMs is essential by investigating the model performance for the present climate; hence, this chapter presents these results. Spatial distributions of the 25-year mean precipitation bias from the large-scale forcing GCM, the five individual RCMs, and MME are shown in Fig. 2. The observed precipitation is characterized by a prominent rainband related to the EASM, which extends along the South China Sea, southern China, the Korean Peninsula, and Japan (Fig. 2a). Each RCM tends to overestimate precipitation in the monsoon rainband around the South China Sea and the East China Sea. Moreover, all RCMs overestimate precipitation over most parts of the western North Pacific. The spatial pattern of precipitation bias over the ocean from each RCM is similar to that from the large-scale forcing GCM, which can be interpreted as the RCM's systematic bias that can be affected by the forcing data. Thus, RCMs overestimate precipitation over the EASM region and the western North Pacific because of the systematic error in the large-scale forcing, which is consistent with the results of Huang and Gao (2018). However, the individual differences of biases between RCMs exist depending on the model configuration such as dynamic cores and physical parameterization schemes. Compared to the forcing data, HadGEM3-RA, RegCM, and SNURCM have smaller biases over land, while other RCMs have more substantial biases, particularly over the ocean and southern China. The result of MME is similar to that of each RCM in terms of spatial pattern; however, the maximum bias of MME, which is offset through the ensemble process, is smaller than that of each RCM.

A more quantitative view of the agreement between each model and observation dataset for 25-year mean precipitation can be obtained from Taylor diagrams (Fig. 3), which show the spatial correlation and the normalized standard deviation. In the case of land, there is a large spread in the standard deviation between models before the bias correction step, while the spread in the spatial correlation is relatively small. In particular, GRIMs has the standard deviation more than twice as large as that of the observations. MME has a slightly higher spatial correlation than all RCMs, which is consistent with the results in Wu et al. (2015), but the standard deviation of MME is at the average level of the other models. Standard deviations of WRF, GRIMs, and MME are much more overestimated than those of the large-scale forcing GCM,

which is related to the larger biases over land compared to the forcing data in Fig. 2. However, the bias correction yields almost identical standardized deviation and spatial correlation to the observed data. Thus, the bias correction can improve the spatial variance and the correlation of long-term mean precipitation. In the case of the ocean, the spatial correlations of all models are lower than those over land. HadGEM2-AO, which is the only coupled ocean-atmosphere model in this study, has the highest spatial correlation. On the other hand, RCMs, which prescribe sea surface temperature data from the large-

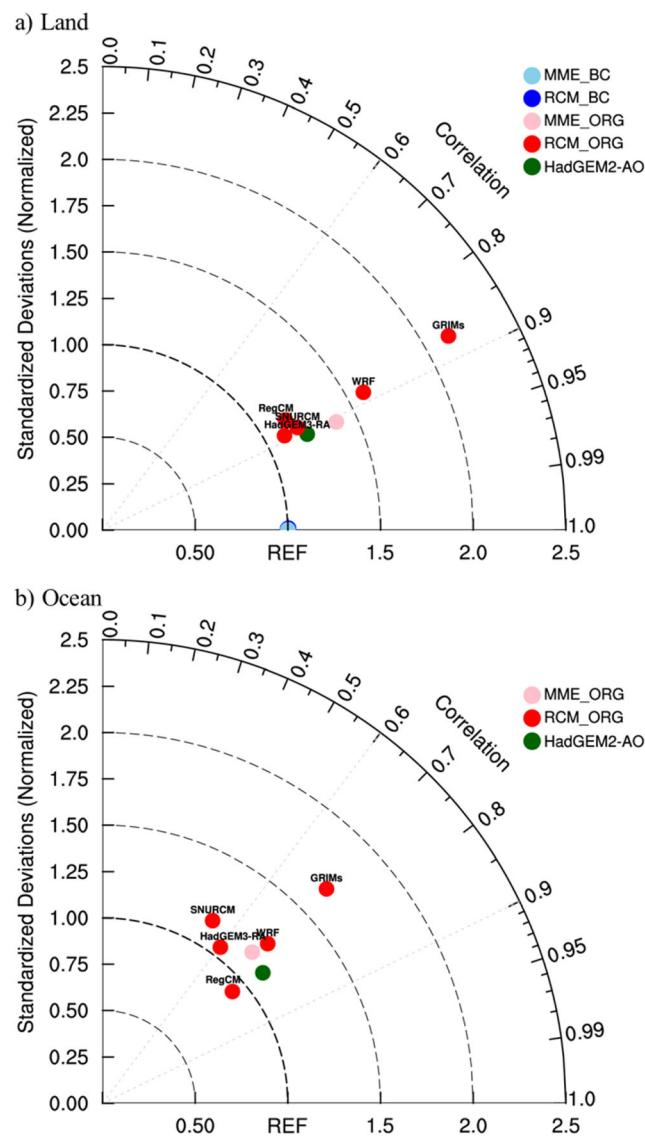


Fig. 3 Taylor diagram of 25-year (1981–2005) mean precipitation in Historical experiment for (a) land and (b) the ocean from the large-scale forcing data, each RCM, and MME. Radial and angular coordinates indicate the magnitude of normalized standard deviation and spatial correlation, respectively. The radial distance from the origin is proportional to the normalized standard deviation of the pattern. Each field is normalized by the corresponding standard deviation of the APHRODITE dataset to be shown. In the legend, “_BC,” and “_ORG” indicate bias-corrected, and non-bias corrected precipitation, respectively

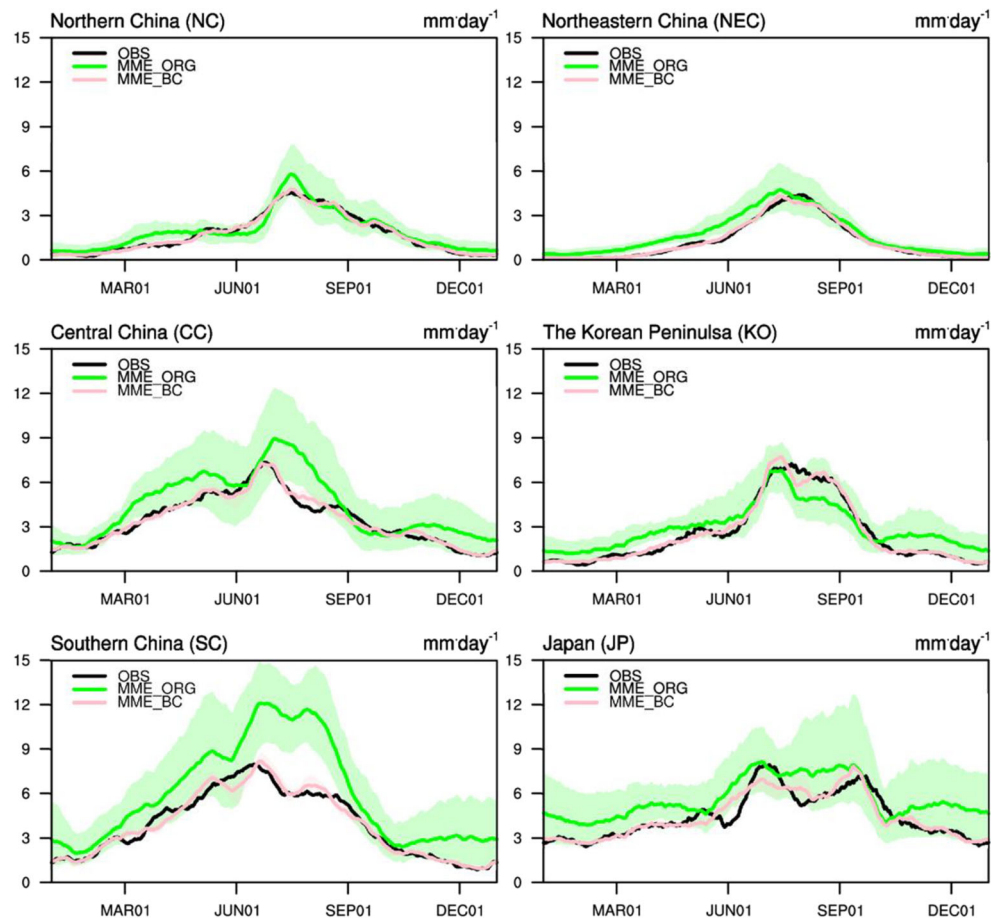
scale forcing data, have relatively low correlations. Contrary to HadGEM2-AO, RCMs are not coupled to the ocean model therefore, reasonable simulation of precipitation over the ocean might be difficult because of the lack of air-sea interactions (Cha et al. 2011; Zhou et al. 2015).

Figure 4 shows the annual cycle of precipitation over the six sub-regions affected by the EASM. A 21-day moving averaging is performed to remove the sub-seasonal signal. Observed precipitation peaks appear during summer in order of SC, CC, JP, KO, and NEC, which is consistent with the EASM onset timing in Wang and LinHo (2002). Moreover, the amounts of precipitation over NC and NEC, which are relatively less affected by the EASM, are less than those over the other regions. However, certain biases exist between MME and observations in the annual cycle of precipitation. Precipitation over SC, CC, and JP, where the onset of the EASM is earlier than that over the other sub-regions, is overestimated during the entire period. Especially over SC, summer precipitation is overestimated by approximately 50%. The spreads between models in summertime annual cycle precipitation in SC, CC, and JP, where the main monsoon-band passes directly are wider (Fig. 2), than those over the other sub-regions, indicating that each RCM simulates the intensity of the EASM differently. Besides, MME simulates

precipitation peaks over SC, CC, and JP later than the peaks noted for the observed data, while the peaks over NEC and KO are simulated earlier than the observed. Also, the results of the annual cycle of bias-corrected precipitation are shown in Fig. 4. In conjunction with the long-term mean precipitation (Fig. 3), the amount, as well as timing of annual cycle precipitation over each region except for JP, is corrected similarly to the observations. Furthermore, spreads between RCMs decrease noticeably during the entire season. Therefore, the bias correction can reduce the model spread regarding future changes in precipitation.

To examine the relationship between precipitation bias and model performance for the EASM, the time-latitude Hovmöller diagram of the 25-year mean low-level meridional wind from May to August is presented in Fig. 5, which shows the intensity and evolution of the EASM. As per the results of ERA-Interim, for $2 \text{ m}\cdot\text{s}^{-1}$ lines, attention is paid to the one peak regime above 25°N from mid-May that reaches its maximum in late-July followed by a retreating phase up to mid-August. Southerly wind over $4 \text{ m}\cdot\text{s}^{-1}$ is the strongest at $20^\circ\text{--}30^\circ\text{N}$ in June. However, the results of HadGEM2-AO (i.e., large-scale forcing data) demonstrate that the southerly wind below 30°N is overestimated. Also, the retreat phase begins approximately 15 days earlier than that of ERA-Interim and

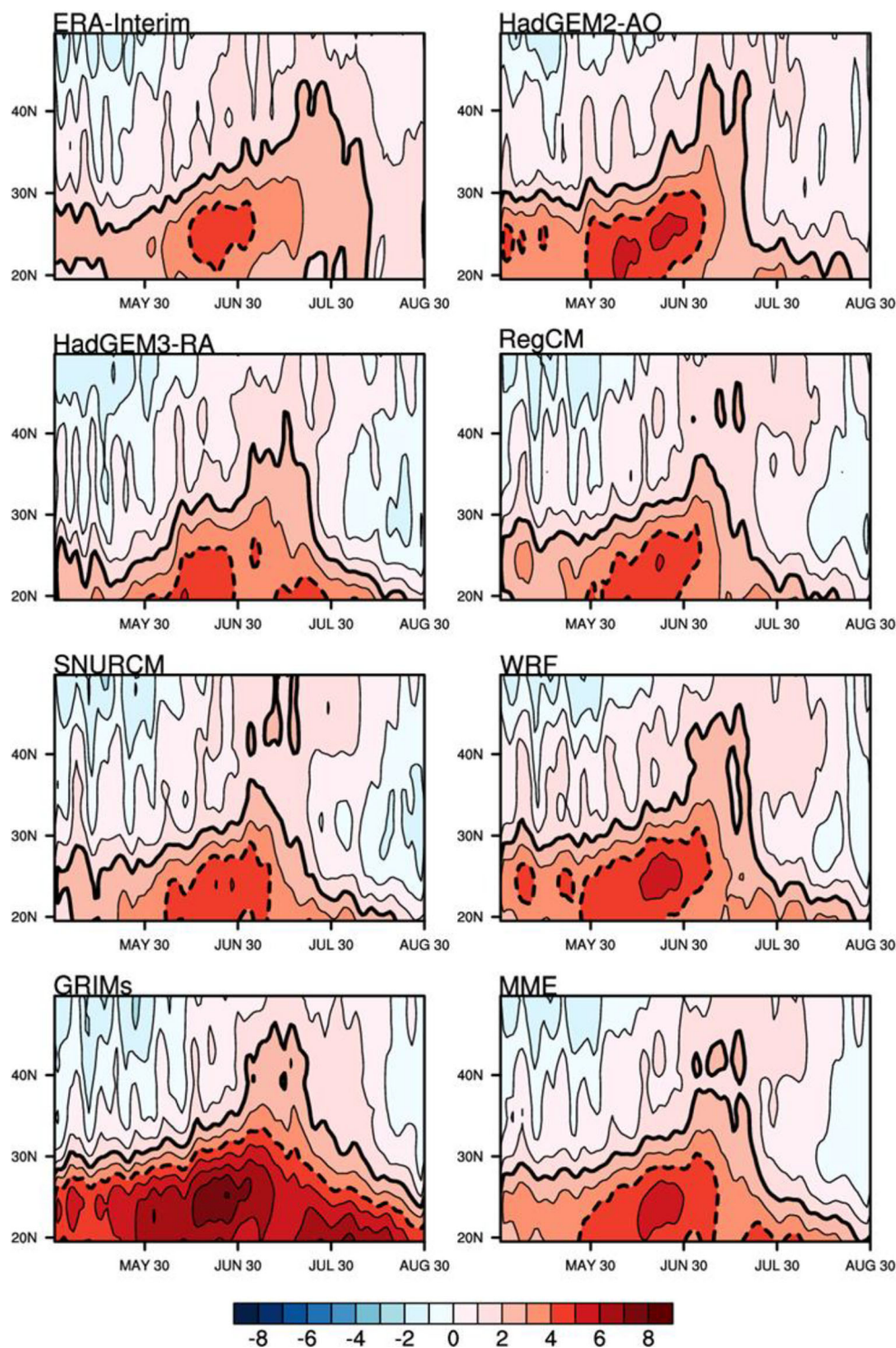
Fig. 4 Annual cycle of area-averaged precipitation ($\text{mm}\cdot\text{day}^{-1}$) with and without bias correction over six sub-regions of MME (green solid/pink solid) and APHRODITE (black solid) in the Historical experiment. Green (pink) areas represent model spread of non-bias corrected (bias-corrected) precipitation between RCMs



proceeds very rapidly. Each RCM and MME have a similar bias feature to the large-scale forcing data. In particular, GRIMs tends to exaggerate southerly wind below 30°N, and RegCM and SNURCM cannot capture the northward march of southerly wind up to 40°N. The low-level meridional wind errors are related to precipitation errors in Fig. 2, implying that precipitation biases over East Asia are affected by the biases of

the EASM. Exaggerated low-level meridional wind below 30°N is associated with the overestimation of precipitation over SC and CC, and the rapid retreat phase of the EASM is related to the early peak phase of precipitation over KO and NEC in Fig. 4. This result elucidates that the model performance to simulate the EASM's timing and intensity must be ensured for reasonable simulation of precipitation over East Asia.

Fig. 5 Hovmöller diagram (time-latitude) of zonally (110° to 140°E) averaged daily meridional wind ($\text{m}\cdot\text{s}^{-1}$) at 850 hPa from ERA-Interim, large-scale forcing data, each RCM and MME in the Historical experiment (1981–2005). The bold solid and dashed line represents 2, 4 $\text{m}\cdot\text{s}^{-1}$, respectively



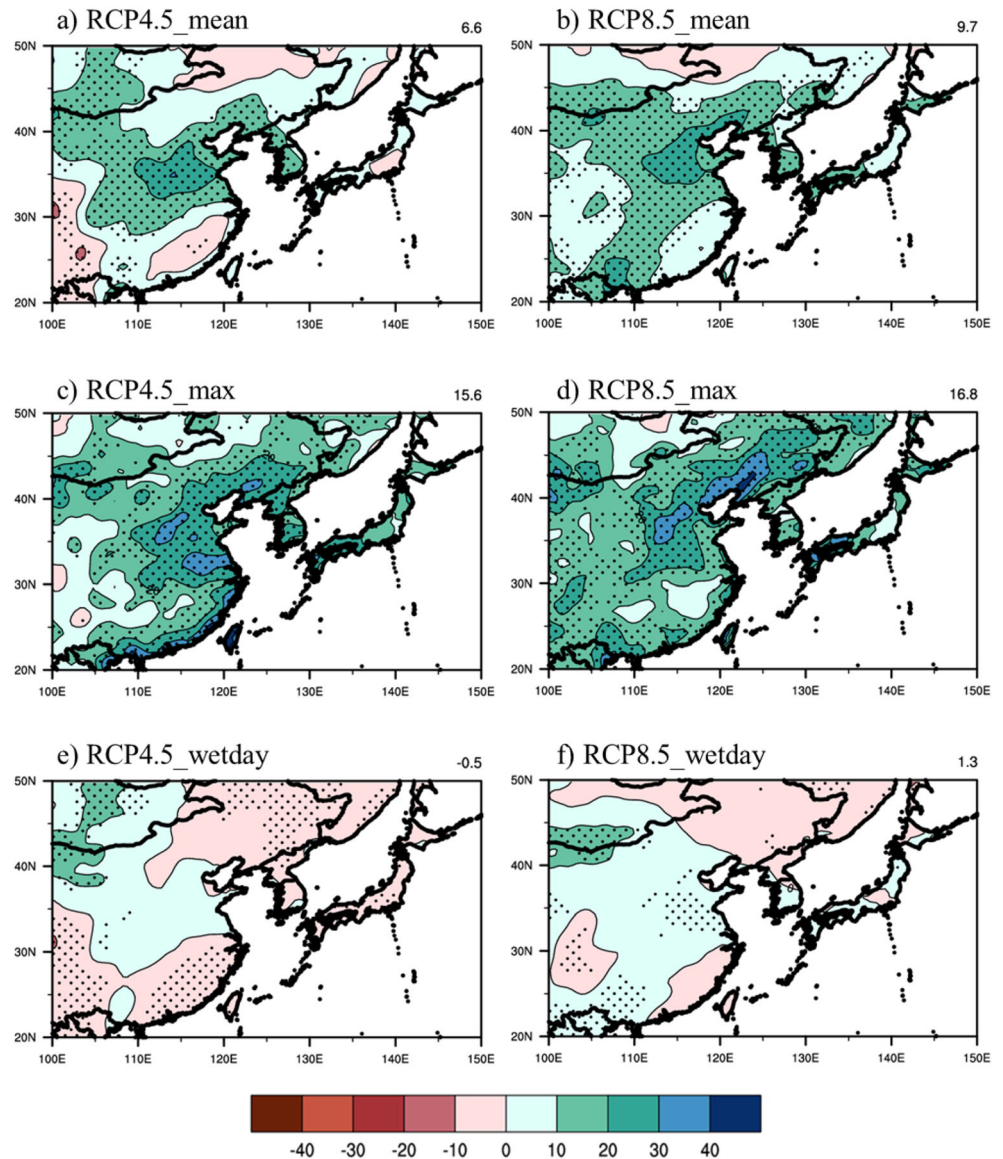
3.2 Projection of the Two RCP Experiments

In this section, we analyze future changes in bias-corrected precipitation between two RCP and historical experiments. Figure 6 shows the rate of precipitation change from MME between the future (2025–2049) and present (1981–2005) periods. Here, a ‘wet day’ is defined as a day when the precipitation amount is more than $1 \text{ mm}\cdot\text{day}^{-1}$. Annual mean precipitation increases over most regions, especially over northern China and the Korean Peninsula in both experiments. However, annual mean precipitation decreases over southern and western China in the RCP4.5 experiment. Annual maximum precipitation also increases over most analysis domain in both RCP scenarios. Increasing trends in future mean and extreme precipitation amounts are consistent with those reported by Kim et al. (2018). In both scenarios, extreme precipitation increases more prominently over most areas

compared to mean precipitation. Area-averaged changes in extreme precipitation are much greater than those in mean precipitation. The ratio of changes in area-averaged mean precipitation compared to those in extreme precipitation is approximately 40% (60%) in the RCP4.5 (RCP8.5) experiment. In contrast to mean and maximum precipitation, changes in annual wetday frequency are not substantial. In the RCP4.5 experiment, the decreasing pattern of annual wetday frequency is dominant, especially over southern China, western China, and northeastern China. In the RCP8.5 experiment, there are also few regions where annual wetday frequency significantly increases. Overall, both mean and extreme precipitation amounts increase compared to wetday frequency regardless of future scenarios, resulting in a greater risk of disasters related to precipitation.

A time-series graph of annual mean precipitation from MME for 69 years (1981–2049) in the selected six sub-

Fig. 6 Rates of changes (%) in (a, b) annual mean daily precipitation amount, (c, d) annual maximum daily precipitation amount, and (e, f) annual wetday frequency from MME between the future (2025–2049) and present (1981–2005) periods. Black dot presents the region that passes the 90% significance t-test. Numbers in the upper right corners indicate area-averaged values



regions is presented (Fig. 7) to analyze the long-term trend of precipitation over East Asia. Under both RCP scenarios, changes in interannual variability (standard deviation) of precipitation over six sub-regions are not significant. However, in all experiments, precipitation over all regions tends to increase gradually. The Mann-Kendall trend test is passed over all regions under the RCP8.5 scenario, while it is only passed over NC, CC, and KO under the RCP4.5 scenario. This implies that annual mean precipitation over NEC, SC, and JP does not have a monotonic increasing trend under the RCP4.5 scenario. The RCP8.5 experiment shows a more prominent increasing trend of precipitation over sub-regions except for NC compared with the RCP4.5 experiment.

Figure 8 shows the annual cycle of precipitation in the two RCP experiments; summer precipitation increases in all regions compared to the Historical experiment. In particular, under the two future scenarios, precipitation over KO and NC considerably increases from July to August. This increment is consistent with the results of changes in mean and extreme precipitation in Fig. 6. Moreover, increasing precipitation in late summer over KO, SC, and JP can be associated with the enhanced typhoon activity in the mid-latitudes (Lee et al. 2019). In summer, precipitation amounts over NC, KO, and CC are much higher in the RCP4.5 experiment than the

RCP8.5 experiment. The reason will be addressed later in Fig. 9. Besides, springtime precipitation over SC, CC, and NC tends to increase in the RCP8.5 experiment, while that over SC in the RCP4.5 experiment does not change significantly due to the large spread between RCMs. Precipitation over JP during fall increases in both RCP experiments despite large uncertainties. No significant changes in winter precipitation are shown over all sub-regions.

Seasonal changes in the atmospheric field are analyzed to understand the sources of change in precipitation (Fig. 9). Increasing greenhouse gases induce atmospheric warming, leading to higher specific humidity as determined by the Clausius-Clapeyron relationship (Ruckstuhl et al. 2007). Thus, the change in low-level humidity can be a thermodynamic factor of precipitation change. Overall, the MME of RCMs projects increasing low-level humidity over most areas every season regardless of the RCP scenarios, which is a favorable condition for increasing precipitation. The increase in low-level moisture is more prominent in summer; it considerably increases over northern China and the Korean Peninsula, where precipitation is significantly increased. SNURCM and WRF project more increasing low-level moisture during summer over inland China in RCP4.5 experiment than in RCP8.5 experiment (not shown), which results in more increasing

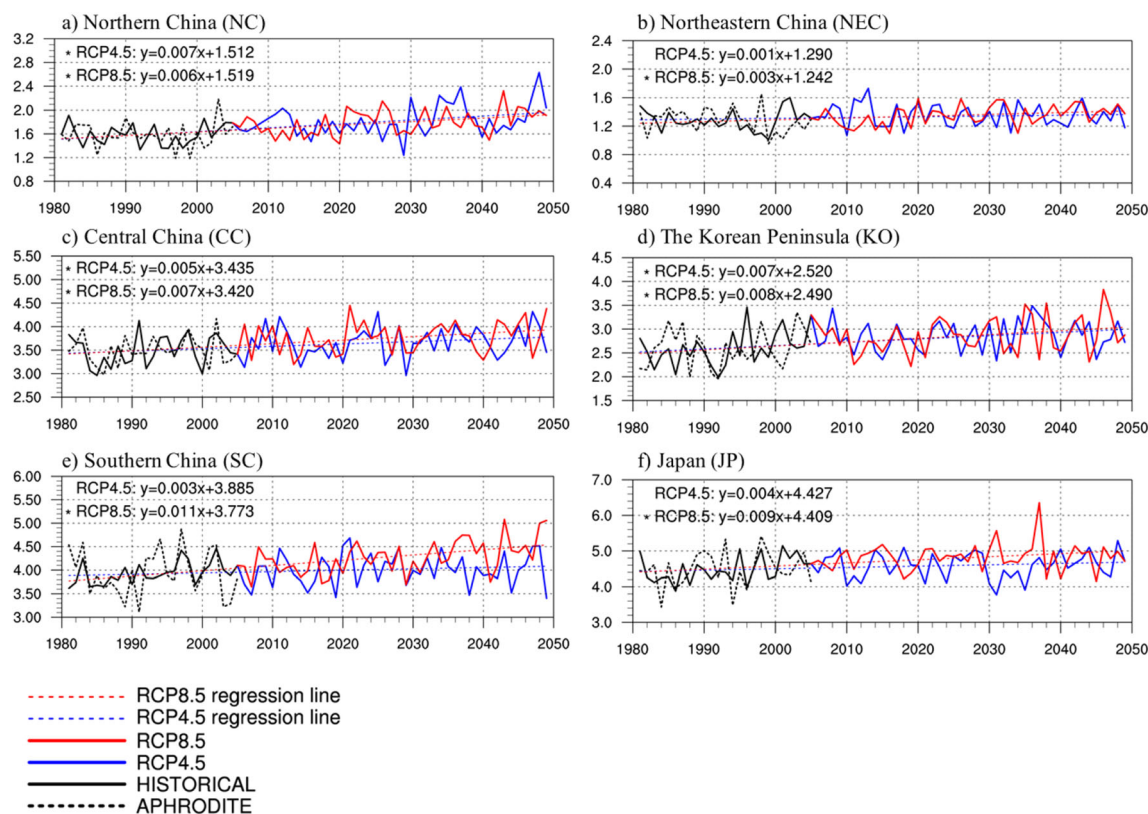


Fig. 7 Time-series (solid) and trend line (dashed) of area-averaged precipitation ($\text{mm}\cdot\text{day}^{-1}$) over the six sub-regions from MME for 69 years (1981–2049) in RCP4.5 (blue) and RCP8.5 (red) experiments. The black dashed line corresponds to the APHRODITE dataset for 25 years (1981–

2005). Equations in the upper left indicate regression equations. The asterisk mark (*) indicates that p value from the Mann-Kendall non-parametric test (Mann 1945; Mondal et al. 2012) is less than 0.05

summertime precipitation over NC, CC, and KO with large spreads between models under RCP4.5 scenarios than under RCP8.5 scenarios in Fig. 8. In contrast to summer, vapors in fall and winter increase more over the ocean than over the land. In particular, the changes in the low-level moisture over the land are smallest in winter which corresponds to a small change in precipitation from Fig. 8. Meanwhile, the precipitation pattern can also be changed by the large-scale circulation as the dynamic factor for precipitation change. In summer affected by the EASM, the southwesterly wind increases over eastern China and the Korean Peninsula under both scenarios owing to the intensified WNPSH. He and Zhou (2015) indicates that HadGEM2-AO, which is used as forcing data in this study, projected an enhanced WNPSH which was dominated by the change in the zonal sea surface temperature gradient between the tropical Indian Ocean and the tropical western Pacific. Thermodynamic and dynamic factors such as increasing

low-level vapor and the intensifying WNPSH lead to favorable conditions for increasing precipitation in summer. In spring, the southwesterly wind is also intensified over eastern China, where precipitation increases under both scenarios. In autumn, in both RCP4.5 and RCP8.5 experiments, increasing northeasterly wind with dry air is dominant in Japan where precipitation increases, which means that there is another important factor for increasing precipitation such as the enhanced typhoon activity in the mid-latitudes (Jin et al. 2016; Lee et al. 2019). In winter, the southerly wind increases over East Asia, but these changes do not lead to an increase in precipitation due to the low amount of vapor.

The time-latitude Hovmöller diagram of changes in the 25-year mean meridional wind at 850 hPa from May to August is presented in Fig. 10. In both RCP experiments, southerly winds prominently increase in July and August. In particular, there is a significant increase

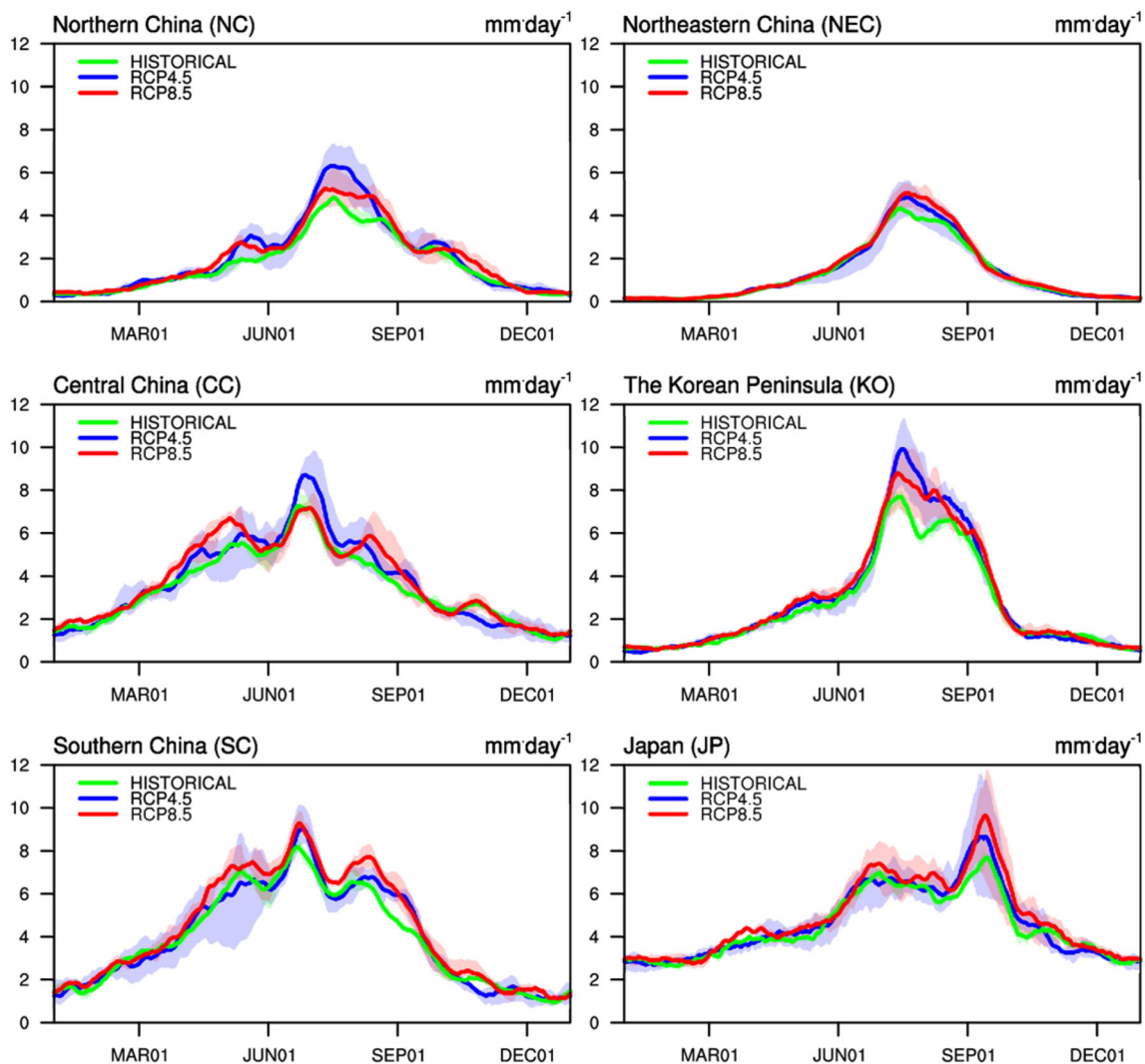


Fig. 8 The annual cycle of area-averaged precipitation (mm day^{-1}) over the six sub-regions of MME in Historical (green), RCP4.5 (blue), and RCP8.5 (red) experiments. Blue and red areas represent model spread between RCMs in RCP4.5 and RCP8.5 experiments, respectively

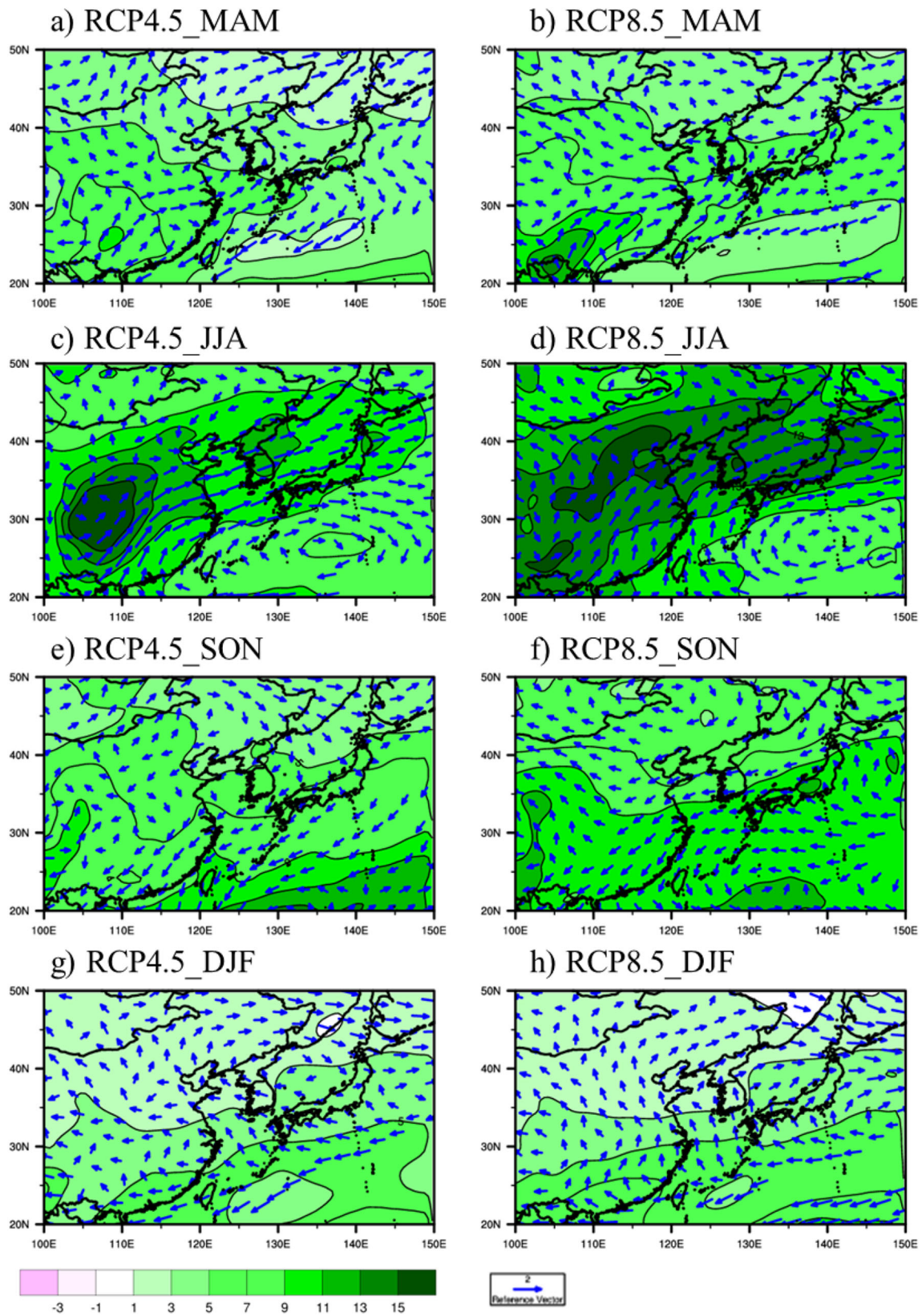


Fig. 9 Seasonal changes in specific humidity ($10^4 \text{ kg}\cdot\text{kg}^{-1}$, shading) and wind ($\text{m}\cdot\text{s}^{-1}$, vector) at 850 hPa between the future (2025–2049) and present (1981–2005) periods from MME in the RCP4.5 (left) and RCP8.5 (right) experiments. Note that specific humidity has high inter-

model consistency over the entire regions, and only wind vectors with good inter-model consistency (more than 4 models having the same sign) are plotted

in the southerly wind within 30°–40°N where northern China (NC) and the Korean Peninsula (KO) are located (Fig. 1), which allows future EASM to move northward while keeping it stronger in the mid-latitudes and staying longer until late summer as compared to present EASM. In other words, regardless of two RCP scenarios, the intensity and the duration of the EASM in the retreat phase is enhanced and extended. The enhanced EASM can be related to the intensification of the WNPSH, as shown in Fig. 9.

3.3 Summary and Conclusions

In this study, a model simulation for the present precipitation was evaluated, and regional precipitation change was analyzed over East Asia using the CORDEX-East Asia Phase I dataset. For the present climate (1981–2005), HadGEM2-AO, which is the large-scale forcing data, tended to overestimate low-level southerly wind below 30°N associated with the EASM. The retreat phase of the EASM simulated by HadGEM2-AO started too early and proceeded very rapidly. Hence HadGEM2-AO overestimated long-term mean precipitation in the monsoon rainband along the East China Sea and the South China Sea. The spatial patterns of biases of RCMs were similar to those of the large-scale forcing data, and detailed biases of RCMs varied according to the model setup. The RCMs overestimated precipitation over the region below 30°N, while they underestimated precipitation within 30–40°N regions in late summer owing to the poor performance of GCM for the EASM. To reduce these systematic biases, power transformation, which is one of the bias correction methods, was applied to daily precipitation data from each RCM. Upon bias correction application, the spatial variability and spatial correlation of long-term mean precipitation became similar to the observed data, and the annual cycle of precipitation was greatly improved; moreover, the spreads between RCMs were also significantly reduced.

Future changes in bias-corrected precipitation under the two RCP scenarios were investigated. In both scenarios, mean and extreme precipitation over most regions increased together compared to the frequency of wetday, especially in the Korean Peninsula and northern China. In particular, the increment of extreme precipitation was greater than that of mean precipitation. Precipitation over all sub-regions affected by the EASM had increasing trends regardless of the RCP scenarios. The intensity and duration of annual precipitation peaks in the two RCP experiments increased over the Korean Peninsula and northern China. The reason for increasing precipitation could be associated with thermodynamic and dynamic factors. Low-level water

vapor as the thermodynamic factor increased every season in the mid-twenty-first century, and the enhanced WNPSH as the dynamic factor during summer resulted in the EASM being reinforced within 30–40°N and staying longer compared to the present climate. The increase in the southerly wind related to the EASM over eastern China and the Korean Peninsula formed favorable conditions for increasing precipitation. In the two RCP experiments, the EASM during the retreat phase was enhanced and extended compared to the Historical experiment. As a result, future summertime precipitation increased significantly over most regions, especially northern China and the Korean Peninsula.

The results of this study imply that the large-scale forcing data with an excellent model performance for the EASM should be selected when simulating climate over East Asia using RCMs. This study also shows that post-processing using bias correction can be valid for

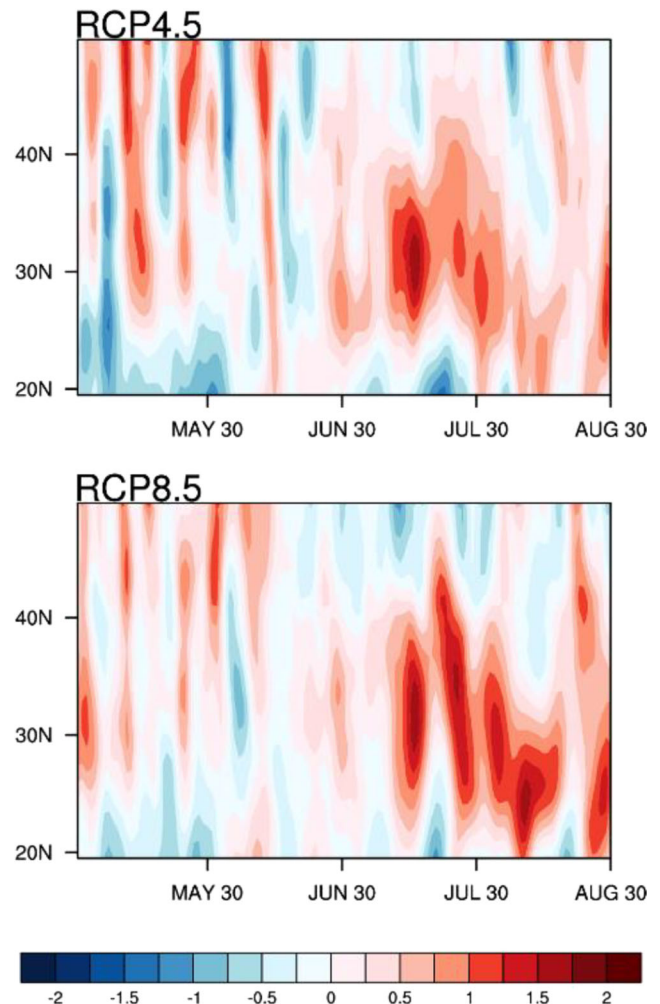


Fig. 10 The Hovmöller diagram (Time×Latitude) of changes in zonally (110° to 140°E) averaged daily meridional wind ($\text{m}\cdot\text{s}^{-1}$) at 850 hPa from MME between two RCP experiments (2025–2049) and the Historical experiment (1981–2005)

estimating more reliable changes in future climate. Finally, the results of changes in precipitation over East Asia can be used as policy basics and input data of other application studies such as hydrology, health, and agriculture. One limitation of the CORDEX-East Asia Phase I dataset is that the lateral boundary conditions generated by a single GCM are deterministically downscaled. The uncertainties regarding future climate projections have to be reduced using an MME approach in which global scenarios generated by multi-GCMs are dynamically downscaled using multi-RCMs to overcome this limitation. As the next step of the CORDEX-East Asia Phase I, the Phase II simulations are under progress that involves dynamic downscaling of multi-GCMs using multi-RCMs with higher resolution.

Acknowledgments This work was funded by the Korea Meteorological Administration Research and Development Program under Grant KMI (KMI2018-01211).

References

- Baek, H.J., Lee, J., Lee, H.S., Hyun, Y.K., Cho, C., Kwon, W.T., Marzin, C., Gan, S.Y., Kim, M.J., Choi, D.H., Lee, J., Lee, J., Boo, K.O., Kang, H.S., Byun, Y.H.: Climate change in the 21st century simulated by HadGEM2-AO under representative concentration pathways. *Asia-Pac. J. Atmos. Sci.* **49**(5), 603–618 (2013). <https://doi.org/10.1007/s13143-013-0053-7>
- Cha, D.H., Lee, D.K.: Reduction of systematic errors in regional climate simulations of the summer monsoon over East Asia and the western North Pacific by applying the spectral nudging technique. *J. Geophys. Res.-Atmos.* **114**(D14), (2009). <https://doi.org/10.1029/2008jd011176>
- Cha, D.H., Jin, C.S., Lee, D.K., Kuo, Y.H.: Impact of intermittent spectral nudging on regional climate simulation using Weather Research and Forecasting model. *J. Geophys. Res.-Atmos.* **116**(D10), (2011). <https://doi.org/10.1029/2010JD015069>
- Christensen, J.H., Machenhauer, B., Jones, R.G., Schar, C., Ruti, P.M., Castro, M., Visconti, G.: Validation of present-day regional climate simulations over Europe: LAM simulations with observed boundary conditions. *Clim. Dyn.* **13**(7–8), 489–506 (1997). <https://doi.org/10.1007/s003820050178>
- Christensen, J.H., Carter, T.R., Rummukainen, M., Amanatidis, G.: Evaluating the performance and utility of regional climate models: the PRUDENCE project. *Clim. Chang.* **81**, 1–6 (2007). <https://doi.org/10.1007/s10584-006-9211-6>
- Corliss, G.: Which root does the bisection algorithm find? *SIAM Rev.* **19**(2), 325–327 (1977). <https://doi.org/10.1137/1019044>
- Curry, J.A., Lynch, A.H.: Comparing Arctic regional climate model. *EOS Trans. Am. Geophys. Union.* **83**(9), 87–87 (2002). <https://doi.org/10.1029/2002eo000051>
- Davies, T., Cullen, M.J.P., Malcolm, A.J., Mawson, M.H., Staniforth, A., White, A.A., Wood, N.: A new dynamical core for the met Office's global and regional modelling of the atmosphere. *Q. J. R. Meteorol. Soc.* **131**(608), 1759–1782 (2005). <https://doi.org/10.1256/qj.04.101>
- Ding, Y.J., Yang, D.Q., Ye, B.S., Wang, N.L.: Effects of bias correction on precipitation trend over China. *J. Geophys. Res.-Atmos.* **112**(D13), (2007). <https://doi.org/10.1029/2006JD007938>
- Dosio, A., Paruolo, P.: Bias correction of the ENSEMBLES high-resolution climate change projections for use by impact models: Evaluation on the present climate. *J. Geophys. Res.* **116**(D16), (2011). <https://doi.org/10.1029/2011jd015934>
- Fu, C.B., Wang, S.Y., Xiong, Z., Gutowski, W.J., Lee, D.K., McGregor, J.L., Sato, Y., Kato, H., Kim, J.W., Suh, M.S.: Regional climate model intercomparison project for Asia. *Bull. Am. Meteorol. Soc.* **86**(2), 257–25+ (2005). <https://doi.org/10.1175/Bams-86-2-257>
- Giorgi, F., Mearns, L.O.: Introduction to special section: Regional climate modeling revisited. *J. Geophys. Res.-Atmos.* **104**(D6), 6335–6352 (1999). <https://doi.org/10.1029/98jd02072>
- Giorgi, F., Jones, C., Asrar, G.R.: Addressing climate information needs at the regional level: the CORDEX framework. *WMO Bull.* **58**(3), 175 (2009)
- Giorgi, F., Coppola, E., Solmon, F., Mariotti, L., Sylla, M.B., Bi, X., Elguindi, N., Diro, G.T., Nair, V., Giuliani, G., Turuncoglu, U.U., Cozzini, S., Guttler, I., O'Brien, T.A., Tawfik, A.B., Shalaby, A., Zakey, A.S., Steiner, A.L., Stordal, F., Sloan, L.C., Brankovic, C.: RegCM4: model description and preliminary tests over multiple CORDEX domains. *Clim. Res.* **52**(1), 7–29 (2012). <https://doi.org/10.3354/cr01018>
- Hall, A.: Climate. Projecting regional change. *Science.* **346**(6216), 1461–1462 (2014). <https://doi.org/10.1126/science.aaa0629>
- Hanel, M., Buishand, T.A.: Analysis of precipitation extremes in an ensemble of transient regional climate model simulations for the Rhine basin. *Clim. Dyn.* **36**(5–6), 1135–1153 (2011). <https://doi.org/10.1007/s00382-010-0822-2>
- He, C., Zhou, T.: Responses of the western North Pacific subtropical high to global warming under RCP4. 5 and RCP8. 5 scenarios projected by 33 CMIP5 models: The dominance of tropical Indian Ocean–tropical western Pacific SST gradient. *J. Clim.* **28**(1), 365–380 (2015). <https://doi.org/10.1175/JCLI-D-13-00494.1>
- Hong, S.Y., Kanamitsu, M.: Dynamical downscaling: fundamental issues from an NWP point of view and recommendations. *Asia-Pac. J. Atmos. Sci.* **50**(1), 83–104 (2014). <https://doi.org/10.1007/s13143-014-0029-2>
- Hong, S.Y., Park, H., Cheong, H.B., Kim, J.E.E., Koo, M.S., Jang, J., Ham, S., Hwang, S.O., Park, B.K., Chang, E.C., Li, H.Q.: The global/regional integrated model system (GRIMs). *Asia-Pac. J. Atmos. Sci.* **49**(2), 219–243 (2013). <https://doi.org/10.1007/s13143-013-0023-0>
- Huang, D.L., Gao, S.B.: Impact of different reanalysis data on WRF dynamical downscaling over China. *Atmos. Res.* **200**, 25–35 (2018). <https://doi.org/10.1016/j.atmosres.2017.09.017>
- Im, E.S., Choi, Y.W., Ahn, J.B.: Robust intensification of hydroclimatic intensity over East Asia from multi-model ensemble regional projections. *Theor. Appl. Climatol.* **129**(3–4), 1241–1254 (2017). <https://doi.org/10.1007/s00704-016-1846-2>
- Jin, C.S., Cha, D.H., Lee, D.K., Suh, M.S., Hong, S.Y., Kang, H.S., Ho, C.H.: Evaluation of climatological tropical cyclone activity over the western North Pacific in the CORDEX-East Asia multi-RCM simulations. *Clim. Dyn.* **47**(3–4), 765–778 (2016). <https://doi.org/10.1007/s00382-015-2869-6>
- Kim, G., Cha, D.H., Park, C., Lee, G., Jin, C.S., Lee, D.K., Suh, M.S., Ahn, J.B., Min, S.K., Hong, S.Y., Kang, H.S.: Future changes in extreme precipitation indices over Korea. *Int. J. Climatol.* **38**, E862–E874 (2018). <https://doi.org/10.1002/joc.5414>
- Kotlarski, S., Keuler, K., Christensen, O.B., Colette, A., Deque, M., Gobiet, A., Goergen, K., Jacob, D., Luthi, D., van Meijgaard, E., Nikulin, G., Schar, C., Teichmann, C., Vautard, R., Warrach-Sagi, K., Wulfmeyer, V.: Regional climate modeling on European scales: a joint standard evaluation of the EURO-CORDEX RCM ensemble. *Geosci. Model Dev.* **7**(4), 1297–1333 (2014). <https://doi.org/10.5194/gmd-7-1297-2014>
- Lee, J.-W., Hong, S.-Y.: Potential for added value to downscaled climate extremes over Korea by increased resolution of a regional climate

- model. *Theor. Appl. Climatol.* **117**(3–4), 667–677 (2014). <https://doi.org/10.1007/s00704-013-1034-6>
- Lee, D.K., Cha, D.H., Kang, H.S.: Regional climate simulation of the 1998 summer flood over East Asia. *J. Meteorol. Soc. Jpn.* **82**(6), 1735–1753 (2004). <https://doi.org/10.2151/jmsj.82.1735>
- Lee, J.W., Hong, S.Y., Chang, E.C., Suh, M.S., Kang, H.S.: Assessment of future climate change over East Asia due to the RCP scenarios downscaled by GRIMs-RMP. *Clim. Dyn.* **42**(3–4), 733–747 (2014). <https://doi.org/10.1007/s00382-013-1841-6>
- Lee, H., Waliser, D.E., Ferraro, R., Iguchi, T., Peters-Lidard, C.D., Tian, B., Loikith, P.C., Wright, D.B.: Evaluating hourly rainfall characteristics over the U.S. Great Plains in dynamically downscaled climate model simulations using NASA-Unifed WRF. *J. Geophys. Res.-Atmos.* **122**(14), 7371–7384 (2017). <https://doi.org/10.1002/2017jd026564>
- Lee, H., Jin, C.-S., Cha, D.-H., Lee, M., Lee, D.-K., Suh, M.-S., Hong, S.-Y., Kang, H.-S.: Future change in tropical cyclone activity over the western North Pacific in CORDEX-East Asia multi-RCMs forced by HadGEM2-AO. *J. Clim.* **2019**, (2019). <https://doi.org/10.1175/jcli-d-18-0575.1>
- Mann, H.B.: Nonparametric Tests against Trend. *Econometrica.* **13**(3), 245–259 (1945). <https://doi.org/10.2307/1907187>
- Martin, G.M., Bellouin, N., Collins, W.J., Culverwell, I.D., Halloran, P.R., Hardiman, S.C., Hinton, T.J., Jones, C.D., McDonald, R.E., McLaren, A.J., O'Connor, F.M., Roberts, M.J., Rodriguez, J.M., Woodward, S., Best, M.J., Brooks, M.E., Brown, A.R., Butchart, N., Dearden, C., Derbyshire, S.H., Dharssi, I., Doutriaux-Boucher, M., Edwards, J.M., Falloon, P.D., Gedney, N., Gray, L.J., Hewitt, H.T., Hobson, M., Huddleston, M.R., Hughes, J., Ineson, S., Ingram, W.J., James, P.M., Johns, T.C., Johnson, C.E., Jones, A., Jones, C.P., Joshi, M.M., Keen, A.B., Liddicoat, S., Lock, A.P., Maidens, A.V., Manners, J.C., Milton, S.F., Rae, J.G.L., Ridley, J.K., Sellar, A., Senior, C.A., Totterdell, I.J., Verhoef, A., Vidale, P.L., Wiltshire, A., Team, H.D.: The HadGEM2 family of Met Office Unified Model climate configurations. *Geosci. Model Dev.* **4**(3), 723–757 (2011). <https://doi.org/10.5194/gmd-4-723-2011>
- Mezghani, A., Dobler, A., Haugen, J.E., Benestad, R.E., Parding, K.M., Piniewski, M., Kardel, I., Kundzewicz, Z.W.: CHASE-PL climate projection dataset over Poland – bias adjustment of EURO-CORDEX simulations. *Earth Syst. Sci. Data.* **9**(2), 905–925 (2017). <https://doi.org/10.5194/essd-9-905-2017>
- Mondal, A., Kundu, S., Mukhopadhyay, A.: Rainfall trend analysis by Mann-Kendall test: a case study of north-eastern part of Cuttack district, Orissa. *Int. J. Geol. Earth Environ. Sci.* **2**(1), 70–78 (2012)
- Monhart, S., Spirig, C., Bhend, J., Bogner, K., Schar, C., Liniger, M.A.: Skill of subseasonal forecasts in Europe: effect of Bias correction and downscaling using surface observations. *J. Geophys. Res.-Atmos.* **123**(15), 7999–8016 (2018). <https://doi.org/10.1029/2017jd027923>
- Ngai, S.T., Tangang, F., Juneng, L.: Bias correction of global and regional simulated daily precipitation and surface mean temperature over Southeast Asia using quantile mapping method. *Glob. Planet. Chang.* **149**, 79–90 (2017). <https://doi.org/10.1016/j.gloplacha.2016.12.009>
- Noguer, M., Jones, R., Murphy, J.: Sources of systematic errors in the climatology of a regional climate model over Europe. *Clim. Dyn.* **14**(10), 691–712 (1998). <https://doi.org/10.1007/s003820050249>
- Park, J.H., Oh, S.G., Suh, M.S.: Impacts of boundary conditions on the precipitation simulation of RegCM4 in the CORDEX East Asia domain. *J. Geophys. Res.-Atmos.* **118**(4), 1652–1667 (2013). <https://doi.org/10.1002/jgrd.50159>
- Pontoppidan, M., Kolstad, E.W., Sobolowski, S., King, M.P.: Improving the reliability and added value of dynamical downscaling via correction of large-scale errors: a Norwegian perspective. *J. Geophys. Res.-Atmos.* **123**(21), 11,875–811,888 (2018). <https://doi.org/10.1029/2018jd028372>
- Powers, J.G., Klemp, J.B., Skamarock, W.C., Davis, C.A., Dudhia, J., Gill, D.O., Coen, J.L., Gochis, D.J., Ahmadov, R., Peckham, S.E., Grell, G.A., Michalakes, J., Trahan, S., Benjamin, S.G., Alexander, C.R., Dimego, G.J., Wang, W., Schwartz, C.S., Romine, G.S., Liu, Z.Q., Snyder, C., Chen, F., Barlage, M.J., Yu, W., Duda, M.G.: THE WEATHER RESEARCH AND FORECASTING MODEL Overview, System Efforts, and Future Directions. *Bull. Am. Meteorol. Soc.* **98**(8), 1717–1737 (2017). <https://doi.org/10.1175/Bams-D-15-00308.1>
- Prudhomme, C., Dadson, S., Morris, D., Williamson, J., Goodsell, G., Crooks, S., Boelee, L., Davies, H., Buys, G., Lafon, T., Watts, G.: Future flows climate: an ensemble of 1-km climate change projections for hydrological application in Great Britain. *Earth Syst. Sci. Data.* **4**(1), 143–148 (2012). <https://doi.org/10.5194/essd-4-143-2012>
- Riahi, K., Rao, S., Krey, V., Cho, C., Chirkov, V., Fischer, G., Kindermann, G., Nakicenovic, N., Rafaj, P.: RCP 8.5—A scenario of comparatively high greenhouse gas emissions. *Clim. Chang.* **109**(1–2), 33–57 (2011). <https://doi.org/10.1007/s10584-011-0149-y>
- Roads, J., Chen, S., Cocke, S., Druryan, L., Fulakeza, M., LaRow, T., Lonergan, P., Qian, J.H., Zebiak, S.: International Research Institute/Applied Research Centers (IRI/ARCs) regional model intercomparison over South America. *J. Geophys. Res.-Atmos.* **108**(D14), (2003). <https://doi.org/10.1029/2002JD003201>
- Ruckstuhl, C., Philipona, R., Morland, J., Ohmura, A.: Observed relationship between surface specific humidity, integrated water vapor, and longwave downward radiation at different altitudes. *J. Geophys. Res.-Atmos.* **112**(D3), (2007). Art. D03302. <https://doi.org/10.1029/2006jd007850>
- Stocker, T.F., Qin, D., Plattner, G.-K., Tignor, M.M., Allen, S.K., Boschung, J., Nauels, A., Xia, Y., Bex, V., Midgley, P.M.: Climate Change 2013: The physical science basis. contribution of working group I to the fifth assessment report of IPCC the intergovernmental panel on climate change. In: Cambridge University Press, (2014)
- Suh, M.S., Oh, S.G., Lee, D.K., Cha, D.H., Choi, S.J., Jin, C.S., Hong, S.Y.: Development of new ensemble methods based on the performance skills of regional climate models over South Korea. *J. Clim.* **25**(20), 7067–7082 (2012). <https://doi.org/10.1175/Jcli-D-11-00457.1>
- Szabó-Takács, B., Farda, A., Skalák, P., Meitner, J.: Influence of Bias correction methods on simulated Köppen–Geiger climate zones in Europe. *Climate.* **7**(2), 18 (2019). <https://doi.org/10.3390/cli7020018>
- Takle, E.S., Gutowski, W.J., Arritt, R.W., Pan, Z.T., Anderson, C.J., da Silva, R.R., Caya, D., Chen, S.C., Giorgi, F., Christensen, J.H., Hong, S.Y., Juang, H.M.H., Katzfey, J., Lapenta, W.M., Laprise, R., Liston, G.E., Lopez, P., McGregor, J., Pielke, R.A., Roads, J.O.: Project to Intercompare Regional Climate Simulations (PIRCS): Description and initial results. *J. Geophys. Res.-Atmos.* **104**(D16), 19443–19461 (1999). <https://doi.org/10.1029/1999jd900352>
- Teutschbein, C., Seibert, J.: Bias correction of regional climate model simulations for hydrological climate-change impact studies: review and evaluation of different methods. *J. Hydrol.* **456**, 12–29 (2012). <https://doi.org/10.1016/j.jhydrol.2012.05.052>
- Thomson, A.M., Calvin, K.V., Smith, S.J., Kyle, G.P., Volke, A., Patel, P., Delgado-Arias, S., Bond-Lamberty, B., Wise, M.A., Clarke, L.E., Edmonds, J.A.: RCP4.5: a pathway for stabilization of radiative forcing by 2100. *Clim. Chang.* **109**(1–2), 77–94 (2011). <https://doi.org/10.1007/s10584-011-0151-4>
- Van der Linden, P., Mitchell, J., editors: ENSEMBLES: Climate change and its impacts—Summary of research and results from the ENSEMBLES project. In: (2009)
- Veijalainen, N., Lotsari, E., Alho, P., Vehvilainen, B., Kayhko, J.: National scale assessment of climate change impacts on flooding

- in Finland. *J. Hydrol.* **391**(3–4), 333–350 (2010). <https://doi.org/10.1016/j.jhydrol.2010.07.035>
- Wang, B., LinHo: Rainy season of the Asian–Pacific summer monsoon*. *J. Clim.* **15**(4), 386–398 (2002). [https://doi.org/10.1175/1520-0442\(2002\)015<0386:RsoTap>2.0.Co;2](https://doi.org/10.1175/1520-0442(2002)015<0386:RsoTap>2.0.Co;2)
- Wang, Y.Q., Leung, L.R., McGregor, J.L., Lee, D.K., Wang, W.C., Ding, Y.H., Kimura, F.: Regional climate modeling: Progress, challenges, and prospects. *J. Meteorol. Soc. Jpn.* **82**(6), 1599–1628 (2004). <https://doi.org/10.2151/jmsj.82.1599>
- Wu, J., Gao, W.J., Xu, Y.L., Pan, J.: Regional climate change and uncertainty analysis based on four regional climate model simulations over China. *Atmos. Oceanic Sci. Lett.* **8**(3), 147–152 (2015). <https://doi.org/10.3878/AOSL20150013>
- Zhou, X., Li, S., Luo, F., Gao, Y., Furevik, T.: Air–sea coupling enhances the east Asian winter climate response to the Atlantic multidecadal oscillation. *Adv. Atmos. Sci.* **32**(12), 1647–1659 (2015)
- Zou, L., Zhou, T., Peng, D.: Dynamical downscaling of historical climate over CORDEX East Asia domain: a comparison of regional ocean–atmosphere coupled model to stand-alone RCM simulations. *J. Geophys. Res.-Atmos.* **121**(4), 1442–1458 (2016). <https://doi.org/10.1002/2015jd023912>

Publisher's Note Springer Nature remains neutral with regard to jurisdictional claims in published maps and institutional affiliations.